

Utilizing niobium plasmonic perfect absorbers for tunable near- and mid-IR photodetection

AHMED FARAG, MONIKA UBL, ANNIKA KONZELMANN, MARIO HENTSCHEL, AND HARALD GIESSEN*

4th Physics Institute, Center for Integrated Quantum Science and Technology IQST, and Research Center SCoPE, University of Stuttgart, Pfaffenwaldring 57, 70569 Stuttgart, Germany
**giessen@pi4.uni-stuttgart.de*

Abstract: With the fast development of single photon-based technologies such as quantum computing and quantum cryptography, conventional avalanche photodiodes as single photon detectors are not the optimum tools anymore. They are currently replaced by Superconducting Nanowire Single Photon Detectors (SNSPDs) based on the superconducting to normal conducting phase transition. The current challenge with SNSPDs lies in overcoming the trade-off between detection efficiency and recovery time. While a large active area will lead to high detection efficiency, the associated high kinetic inductance causes a long recovery time. Plasmonic effects can play an important role in the absorption enhancement of SNSPDs. Nanostructuring with a suitable geometry can provide a high-absorption cross-section at the intrinsic nanowire surface plasmon resonance, which can be significantly larger than their geometric cross-section. We present a photodetector based on the intrinsic localized surface plasmon resonance of a niobium nanowire, which is one of the common superconductors with low kinetic inductance. Additionally, we are increasing the absorption of our nanostructures even further using a plasmonic perfect absorber scheme. We fabricated a plasmonic perfect absorber superconducting photodetector, investigated its response to external light at resonance, and proved its plasmonic behavior as evidenced by its polarization dependence.

© 2019 Optical Society of America under the terms of the [OSA Open Access Publishing Agreement](#)

1. Introduction

Single-photon based applications such as quantum computing [1,2] and quantum cryptography [3,4] require photon detection with high efficiency and precision. Superconducting Nanowire Single Photon Detectors (SNSPDs) [5] have thus become an interesting field of research [6]. There is usually a trade-off between the detection efficiency and the recovery time of SNSPDs [7,8]. On the one hand, a large photon-active area with long wire will lead to high detection efficiency. On the other hand, long wires exhibit high kinetic inductance, which will lead to long recovery times [9,10]. Plasmonic resonances, with their large resonant absorption cross section, have been brought forward as an effective way to increase the efficiency of SNSPDs.

The absorption efficiency ($\eta_{\text{absorption}}$) is determined by the ability of the detector to absorb the incident photon and trigger a signal; therefore, the design and the material of the detector matters. Many methods have been implemented in order to enhance the absorption efficiency of the SNSPDs such as optical cavities along with anti-reflection coatings [11], waveguides [12,13], and optical nanoantennas [14,15].

The interaction of light with metallic nanostructures reveals unique optical properties originating from the excitation of localized surface plasmons [16,17], which can be used for many applications [18,19]. Hence, plasmonics is expected to play a very important role in enhancing the detection efficiency of SNSPDs, due to the large absorption cross-section at resonance. Moreover, maintaining a small active area of the detector would shorten the recovery time.

Further absorption enhancement for the plasmonic nanostructures could be obtained using the so called plasmonic perfect absorbers, which exhibit a very large absorbance cross-section even at high incidence angles (i.e., at a large numerical aperture) [20]. Gold perfect absorbers were used as plasmonic sensors for refractive index sensing [21]; palladium perfect absorbers for gas sensing applications [22]. Many superconducting materials have been used to fabricate SNSPD such as NbN [23–25], NbTiN [26–28], MoSi [29,30], and WSi [31]. Here we study niobium perfect absorbers to implement them in SNSPDs aiming for perfect absorption using a small active area. Niobium is also one of the common superconductors with low kinetic inductance [32], thus it is attractive material for SNSPDs. It also exhibits good plasmonic properties in the near- and mid-infrared spectral range [33].

First, we study the sputtering parameters that yield the highest quality Nb films in terms of the electrical and optical properties. We fabricate 1D Nb gratings and study their plasmonic properties by exciting localized surface plasmons along the short wire axis (Fig. 1(a)). We then investigate the tunability of the plasmon resonance wavelength as a function of the wire width. Further absorption enhancement is obtained using Nb plasmonic perfect absorber structures (Fig. 1(b)). We use scattering matrix simulations to obtain the structure parameters that yield the maximum absorption, and we use these parameters to fabricate Nb perfect absorbers [34,35]. We fabricate a perfect absorber Nb meander connected to four pad contacts and characterize its superconducting and plasmonic properties (Fig. 1(c)). We put the system in a superconducting state, expose it to external light where its maximum absorption occurs, and prove that the response is indeed plasmonic in nature (Fig. 1(d)).

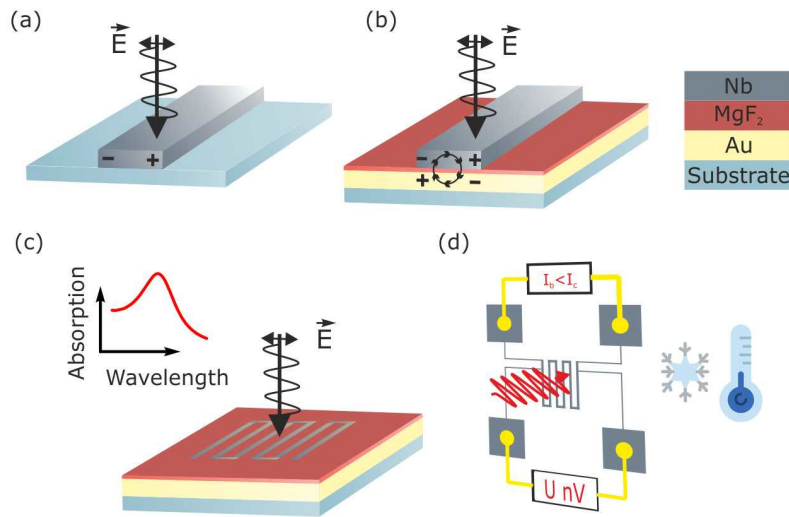


Fig. 1. (a) Schematic illustration of a Nb nanowire on a substrate with the electric field exciting particle plasmons along the short wire axis. (b) Schematic illustration of a Nb plasmonic perfect absorber. Mirror plasmons are generated on the gold mirror surface leading to a circular current and a magnetic response. (c) By optimizing the structure parameters of the Nb perfect absorber, a close to unity absorption could be achieved. (d) Schematic drawing of a perfect absorber SNSPD with a small active area responding to the incident light.

2. Nb sputtering and nanofabrication

Sputtering high quality superconducting Nb films requires high precision before, during, and after deposition. The amount of impurities incorporated into the film degrade its quality, hence contamination control is necessary. To minimize the fraction of impurities, one needs to decrease the number of impurity atoms hitting the film by choosing a highly pure target, maintaining a clean chamber, and depositing in a good vacuum condition. It turned out that

increasing the deposition rate either by increasing the sputtering power and/or decreasing the substrate to target distance leads to high quality films due to minimizing the fraction of impurities [36].

We studied carefully the effect of each of the deposition parameters on the superconducting transition temperature of the Nb films (power, substrate to target distance, background pressure, argon pressure, substrate dependence, and deposition rate). After yielding the optimum deposition parameters that result in high quality Nb films (the exact optimized conditions are given below), we checked the reproducibility by applying these parameters at four subsequent sputtering processes with unchanged conditions. The transition temperature of the films was determined using mutual inductance measurements. As shown in Figs. 2(a) and 2(b), the real and imaginary parts of the mutual inductance indicate the reproducibility of the transition temperature. We are interested in the plasmonic properties of Nb as well, hence, the reproducibility of the optical properties is also worth checking. Modeled spectroscopic ellipsometry measurements were carried out to determine the optical properties of the films in terms of the real and imaginary parts of the dielectric function as shown in Figs. 2(c) and 2(d). The data indicates the reproducibility of the optical properties as well.

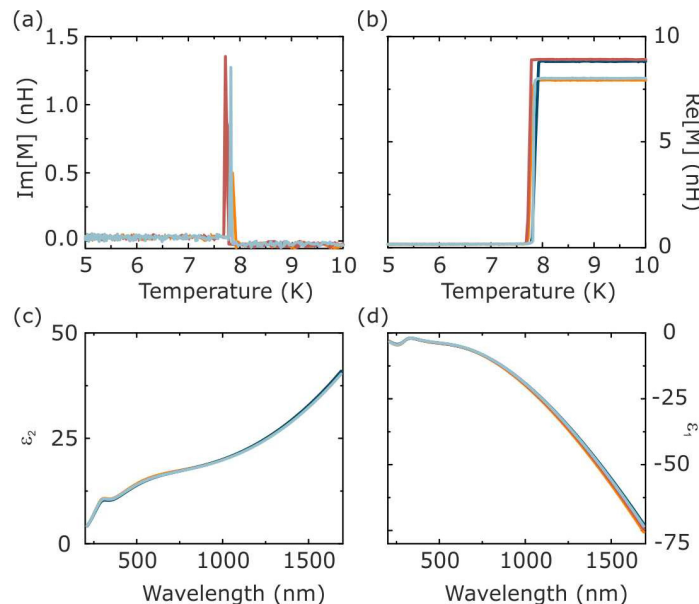


Fig. 2. Reproducibility of the electrical and optical properties of Nb films. Four different 100 nm Nb films were deposited over c-plane sapphire substrates (indicated by different colors) using DC magnetron sputtering. The films were characterized by mutual inductance measurements to determine the superconducting transition temperature ((a) and (b)). Modeled spectroscopic ellipsometry measurements were carried out to determine the optical properties of the films in terms of the real (d) and imaginary (c) parts of the dielectric function. These values were used for our simulations afterwards.

The substrates in the four different processes were c-plane sapphire to exclude the substrate dependence of the film quality [37]. They were cleaned in acetone and propanol for 10 minutes each using an ultrasonic bath at $T = 55^\circ\text{C}$ and $P = 110\text{ Watts}$. The substrates were mounted inside the Pfeiffer 570 sputtering machine and the chamber was pumped for 5 hours; the background pressure was 10^{-7} mbar afterwards. An argon flow rate of 25 sccm was used and this value led to a pressure of 6×10^{-3} mbar. With a DC magnetron sputtering process, we

ignited the plasma using 150 Watts of power and etched the native oxide layer on the target surface for 10 minutes before opening the shutter. The power used during deposition was 600 Watts, which gave a deposition rate of $R = 7.7$ nm/sec considering a constant substrate to target distance.

To study the plasmonic properties of niobium (as well as Nb plasmonic perfect absorbers), we fabricate 1D Nb gratings using electron beam lithography. For the Nb plasmonic perfect absorber we clean the glass substrates in acetone and propanol for 10 minutes each using an ultrasonic bath at $T = 55^\circ\text{C}$ and $P = 110$ Watts. A 5 nm Cr layer is evaporated first using an electron-gun evaporator to enhance the adhesion between the glass substrates and the thick gold mirror evaporated afterwards. A MgF_2 layer is evaporated on top of the Au mirror and annealed for four hours at 400°C to enhance the surface morphology. As shown in Fig. 3(a), the Nb thin film is subsequently sputtered over the multilayer structure (substrate, gold mirror, and spacer layer). A negative photoresist is spun, baked, exposed using electron beam lithography to create the structures of interest, and developed as depicted in Fig. 3(b). The pattern is then transferred to the Nb film below using plasma etching (with an argon-freon mixture) process as shown in Fig. 3(c). Finally, the residual photoresist is dissolved by immersing the sample in NEP solution, producing precise structure dimensions as shown Fig. 3(d).

Laser Interference Lithography (LIL) is one of the common methods used to tailor 1D and 2D plasmonic nanostructures [38–40]. The interference pattern of a UV laser is transferred to a negative-UV sensitive photoresist, followed by transferring the created pattern to the film after developing and a subsequent plasma etching processes. In addition to the electron beam lithography, LIL can be used to fabricate Nb plasmonic perfect absorbers.

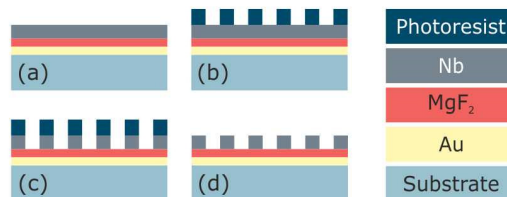


Fig. 3. Schematic drawings of the perfect absorber nanofabrication process using electron beam lithography. (a) 20 nm Nb films are sputtered over the multilayer structure. (b) A negative photoresist is spin coated, exposed using standard electron beam lithography, and developed afterwards. (c) The pattern is transferred to Nb using a reactive ion beam etching process. (d) The residual photoresist is removed by immersing the sample in NEP solution.

3. Nb plasmonics and plasmonic perfect absorbers

As shown Fig. 4 we study the plasmonic properties of our Nb nanostructures. A schematic diagram of a 1D 20 nm thick Nb grating, with the electric field exciting plasmons along the short wire axis, is presented in Fig. 4(a). Simulations, depicted in Fig. 4(b), show that the resonance frequencies of the metallic nanostructures are tunable by their geometrical dimensions. As we excite plasmons along the short wire axis, the plasmon resonance wavelength can be tuned by changing the wire width. These results are corroborated by transmission FTIR measurements shown in Fig. 4(c) for different fields with different wire width. They also demonstrate the tunability of the plasmon resonance wavelength in the IR range. SEM images of the corresponding fields are displayed in Fig. 4(d).

At the telecom wavelength, the Nb plasmonic nanostructures have up to 40% relative transmission. The modulation depth in the relative transmission spectra includes the absorbed, reflected, and scattered light. For our application, only absorbed photons are the ones that

count as they will trigger a detection signal, hence, improved absorption enhancement for the Nb plasmonic nanostructures is still required.

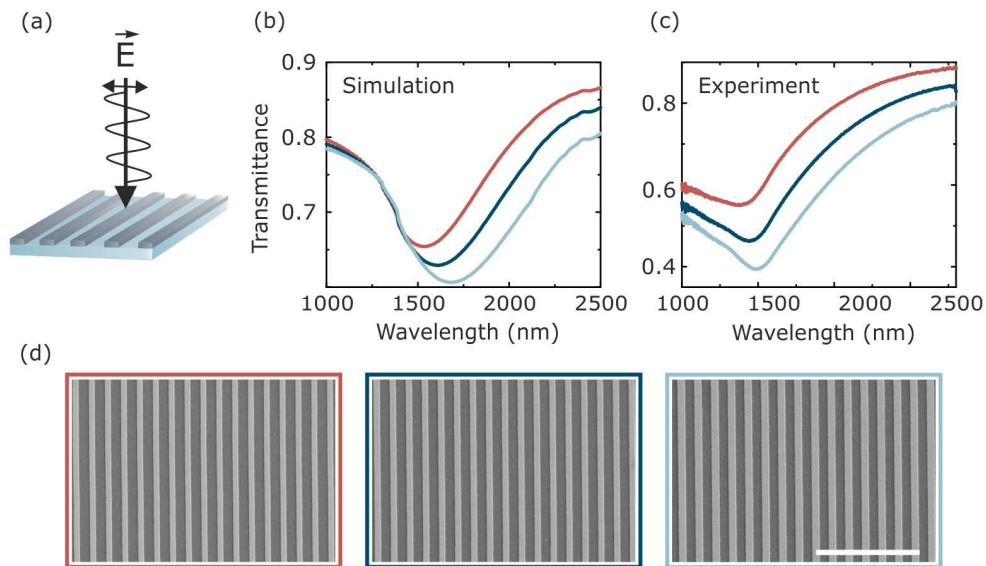


Fig. 4. (a) 20 nm thick Nb nanowires exhibit tunable particle plasmon resonance. We excite plasmons along the short wire axis, hence the resonance wavelength is tunable as a function of the wire width. (b) Simulated spectra of Nb plasmonic nanostructures using scattering matrix. (c) Relative transmission FTIR spectrum. (d) SEM images of the corresponding fields. The wire width from left to right is $W = 260, 290, 330$ nm with a periodicity of 750 nm, the scale bar is 5 μm .

The perfect absorber scheme is a well-known method for enhancing the absorption of plasmonic nanostructures. By using a thick gold mirror, one can block the transmission of the incident light. Choosing the optimum structure parameters (wire width, periodicity, and spacer layer thickness) that lead to impedance matching between the structure and the vacuum, will suppress the reflection [20–22], and the absorption efficiency of the incident light can approach unity. In Fig. 5(a), a schematic drawing of the Nb plasmonic perfect absorber is depicted. The localized surface plasmons are excited along the short wire axis. We use scattering matrix simulations before the nanofabrication process. We run the simulations over wide range of wire widths for different periodicities and different spacer layer thickness. After yielding the optimum structure parameters that result in a perfect absorption around the wavelength of interest as shown in Fig. 5(b), we fabricate 20 nm thick Nb perfect absorbers using electron beam lithography. The relative reflection FTIR measurements in Fig. 5(c) demonstrate the tunability of the particle plasmon resonance as a function of the wire width and 95% absorption. In addition to the high absorption cross section and the wavelength tunability, the plasmonic perfect absorbers tolerate a large range of incident angles, yielding a high numerical aperture upon strong focusing of the incident light [21,22]. A close to unity absorption even with an incident angle of $\theta = 50^\circ$ could be achieved in TM polarization perpendicular to the wires [41].

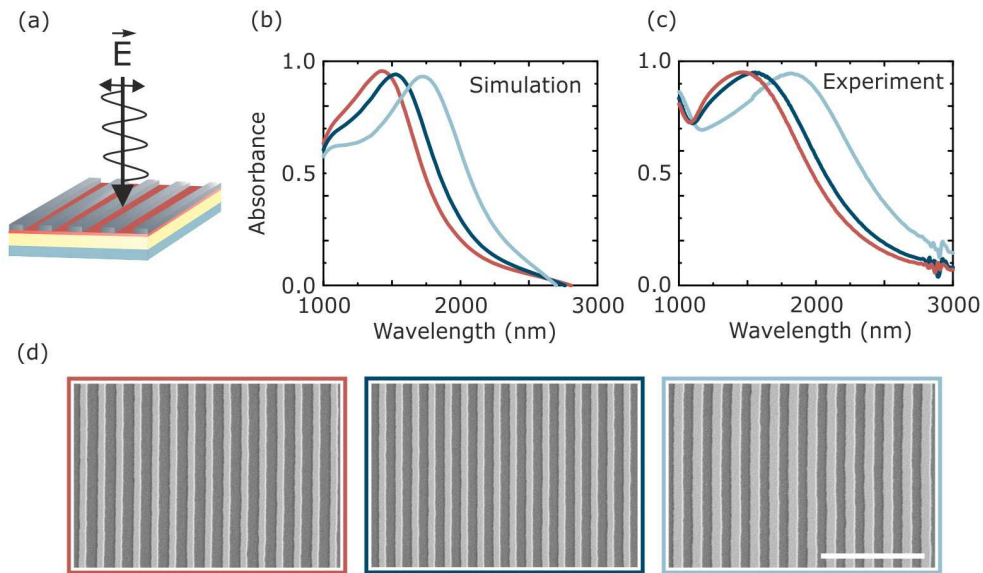


Fig. 5. (a) Schematic drawing of 20 nm thick Nb perfect absorber, with the electric field exciting plasmons along the short wire axis. (b) Absorption spectra for Nb perfect absorbers simulated using scattering matrix. (c) The measured data for the fabricated samples confirms the tunability of the plasmon resonance wavelength and a close to unity absorption at resonance. The wire width from left to right is $W = 270, 290, 340$ nm, and the periodicity is $P = 750$ nm. (d) SEM images for the corresponding fields, the scale bar is 5000 nm.

4. Detector fabrication and characterization

For the perfect absorber superconducting photodetector, a 100 nm Nb film is sputtered over a perfect absorber structure. The detector is fabricated using electron beam lithography. The detector active area is a $10 \times 10 \mu\text{m}^2$ meander (Fig. 6(c)). The wire width is 320 nm with a periodicity of $1 \mu\text{m}$. The meander is connected to four pad contacts (from Nb as well) with sizes $50 \times 50 \mu\text{m}^2$ each (Fig. 6(a)). A relative reflection FTIR measurement was performed to obtain the absorption spectrum of the active area for both parallel and perpendicular polarizations (Fig. 6(d)). For the polarization angle $\varphi = 0^\circ$, the electric field is exciting localized surface plasmons along the short wire axis, and we obtain up to 70% absorption at the resonance wavelength ($\lambda = 1150$ nm). For the perpendicular polarization with $\varphi = 90^\circ$ the absorption is about 20% at the same wavelength. Four aluminum wires are bonded from the four pads to a chip carrier. A four-point resistivity measurement with $I_{\text{bias}} = 50 \mu\text{A}$ is performed from room temperature down to 2K to determine the superconducting transition temperature of the detector, which is 7.5K as indicated in Fig. 6(b).

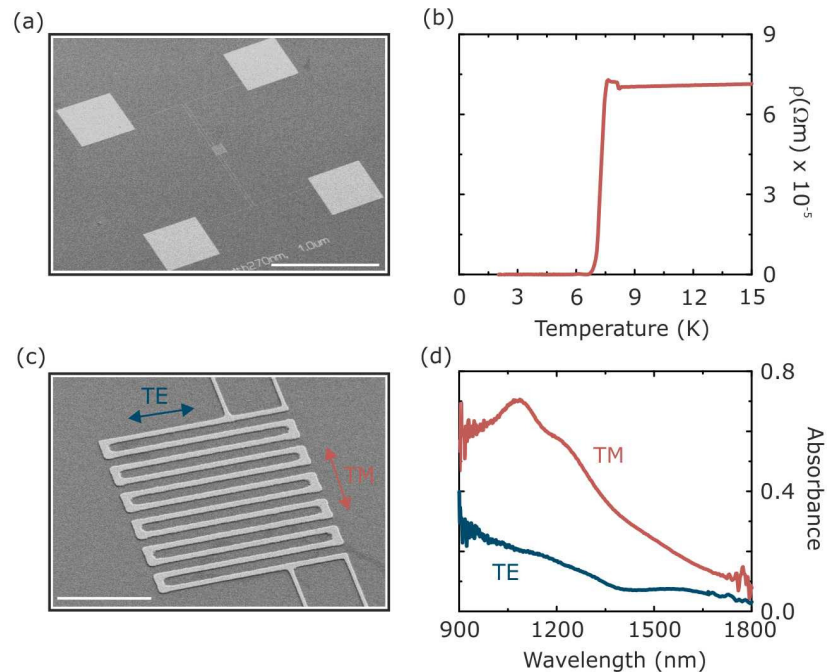


Fig. 6. (a) SEM image of the perfect absorber detector fabricated using electron beam lithography. The active area is connected to four pad contacts (from Nb as well) on top of perfect absorber structure. The scale bar is 100 μm . (b) The detector superconducting transition temperature is determined by performing four-point resistivity measurement and amounts to 7.5 K. (c) SEM image of the active area ($10 \times 10 \mu\text{m}^2$). The total wire length is 130 μm , with 100 nm thickness, 320 nm width, and periodicity 1 μm . The scale bar is 5 μm . (d) FTIR relative reflection measurement for the detector active area to obtain its absorption spectrum. Red indicates the E-field of the incident light polarized along the short axis (TM, $\varphi = 0^\circ$), and blue indicates polarization of E-field along the long axis (TE, $\varphi = 90^\circ$). No plasmonic enhancement is visible in the latter geometry.

To investigate the detector response to external light and investigate the plasmonic role in its absorption behavior, we use a cryostat with optical axis along with a KEITHLEY 2611B current source. For the readout circuit we use a KEITHLEY 2182A nanovoltmeter. The detector is kept in a superconducting state at $T = 6\text{K}$, which is below the transition temperature, and a bias current of $I_{\text{bias}} = 0.95 I_c$. The laser source Toptica ECDL Pro with $\lambda = 1142 \text{ nm}$ (where the maximum absorption occurs) and output power 40 mW is attenuated using neutral density filters. Using a polarizer and a half wave plate we keep the polarization and the power of the incident light well defined. We check the detector response (represented by the voltage drop over the active area) for a wide range of power at TM polarization ($\varphi = 0^\circ$), where the maximum absorption is expected due to the plasmonic effect and at TE polarization ($\varphi = 90^\circ$) where the absorption is expected to be minimum. The results in Fig. 7(c) confirm the polarization dependence of the detector response which proves the plasmonic role in the absorption behavior of the detector. The TM and TE responses are distinguishable from each other for a certain incident power range. For high incident laser power, the power dissipation is too high for both the parallel and perpendicular polarization and the system will transform completely from a pure superconducting state to a pure normal conducting state, i.e., $V(P > 60 \mu\text{W}) = V(T > T_c)$.

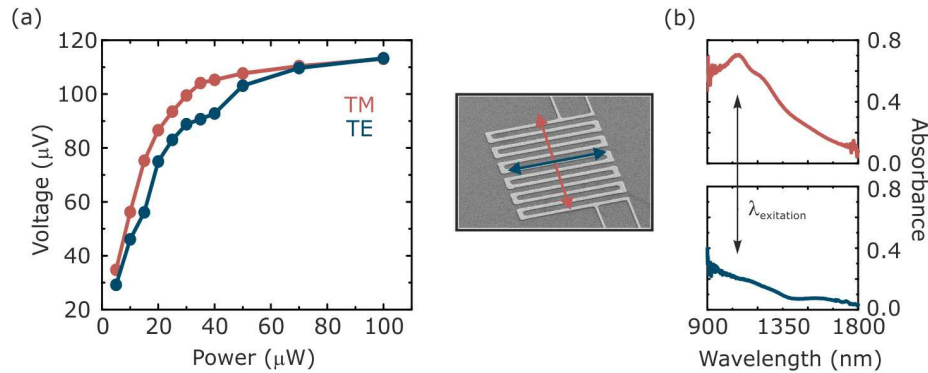


Fig. 7. (a) The detector response for $\lambda = 1142$ nm represented by the voltage drop is measured over a wide power range for both polarization angles. For high power, the response is indistinguishable because the system transforms completely to a normal conducting state. The results indicate the polarization dependence of the detector response and prove that it is plasmonic. (b) FTIR absorption spectrum for the detector active area when the polarization angle is $\phi = 90^\circ$ (TE) and the polarization angle is $\phi = 0^\circ$ (TM). The absorption is maximum in this case due to the plasmonic excitation along the short wire axis.

5. Conclusion and outlook

In summary, we studied the plasmonic properties of Nb as one of the attractive superconductors for superconducting nanowire single photon detectors. Further absorption enhancement for Nb plasmonic nanostructures was carried out using a plasmonic perfect absorber scheme. We use scattering matrix simulations to yield the structure parameters that result in a maximum absorption at the wavelength of interest. We fabricated Nb nanowire plasmonic perfect absorbers using electron beam lithography. We were able to obtain up to 95% absorption at resonance. We fabricated a perfect absorber detector with a small active area. Using a cryostat with optical access we put the system into a superconducting state, exposed it to external light, and proved that the response is polarization dependent. The results agree with the polarization dependence of the absorption behavior for the nanostructure due to the plasmonic effect. In future, we will optimize the perfect absorber detector parameters further to obtain a close to unity absorption for a small active area, which will consequently decrease the detector recovery time. Also, we are developing the supply and read out circuits for our setup to determine the metric parameters of the plasmonic based detector such as the detection efficiency, the recovery time, the dark count rate, and the jittering time. Finally, we should be able to demonstrate single photon detection over a large spectral range in the near- and mid-infrared with enhanced properties compared to state of the art systems.

Funding

European Research Council (ERC) (Complexplas); Deutsche Forschungsgemeinschaft (DFG) (SPP1839, SPP1929); Baden-Württemberg Stiftung; Ministerium für Wissenschaft, Forschung und Kunst Baden-Württemberg (MWK) (IQST, ZAQuant); Open Access Fund University of Stuttgart.

Acknowledgments

We thank Roland Rösslhuber and Ievgen Voloshenko at the 1st Physics Institute for help with ellipsometry, Rostyslav Semenyshyn at the 4th Physics Institute (University of Stuttgart) for the help with FTIR measurements. Also we thank Dr. Gennady Logvenov, Marion Hagel, and Roberto Ortiz at the Max Planck Institute for Solid State Research for their help with Al wire bonding and superconductivity measurements.

References

1. J. L. O'Brien, "Optical quantum computing," *Science* **318**(5856), 1567–1570 (2007).
2. E. Knill, R. Laflamme, and G. J. Milburn, "A scheme for efficient quantum computation with linear optics," *Nature* **409**(6816), 46–52 (2001).
3. H.-K. Lo, M. Curty, and K. Tamaki, "Secure quantum key distribution," *Nat. Photonics* **8**(8), 595–604 (2014).
4. K. Takemoto, Y. Nambu, T. Miyazawa, Y. Sakuma, T. Yamamoto, S. Yorozu, and Y. Arakawa, "Quantum key distribution over 120 km using ultrahigh purity single-photon source and superconducting single-photon detectors," *Sci. Rep.* **5**(1), 14383 (2015).
5. C. M. Natarajan, M. G. Tanner, and R. H. Hadfield, "Superconducting nanowire single-photon detectors: physics and applications," *Supercond. Sci. Technol.* **25**(6), 063001 (2012).
6. G. N. Gol'tsman, O. Okunev, G. Chulkova, A. Lipatov, A. Semenov, K. Smirnov, B. Voronov, A. Dzardanov, C. Williams, and R. Sobolewski, "Picosecond superconducting single-photon optical detector," *Appl. Phys. Lett.* **79**(6), 705–707 (2001).
7. D. Rosenberg, A. J. Kerman, R. J. Molnar, and E. A. Dauler, "High-speed and high-efficiency superconducting nanowire single photon detector array," *Opt. Express* **21**(2), 1440–1447 (2013).
8. A. J. Kerman, E. A. Dauler, J. K. W. Yang, K. M. Rosfjord, V. Anant, K. K. Berggren, G. N. Gol'tsman, and B. M. Voronov, "Constriction-limited detection efficiency of superconducting nanowire single-photon detectors," *Appl. Phys. Lett.* **90**(10), 101110 (2007).
9. A. J. Kerman, E. A. Dauler, W. E. Keicher, J. K. W. Yang, K. K. Berggren, G. Gol'tsman, and B. Voronov, "Kinetic-inductance-limited reset time of superconducting nanowire photon counters," *Appl. Phys. Lett.* **88**(11), 111116 (2006).
10. R. Meservey and P. M. Tedrow, "Measurements of the kinetic inductance of superconducting linear structures," *J. Appl. Phys.* **40**(5), 2028–2034 (1969).
11. K. M. Rosfjord, J. K. W. Yang, E. A. Dauler, A. J. Kerman, V. Anant, B. M. Voronov, G. N. Gol'tsman, and K. K. Berggren, "Nanowire single-photon detector with an integrated optical cavity and anti-reflection coating," *Opt. Express* **14**(2), 527–534 (2006).
12. M. K. Akhlaghi, E. Schelew, and J. F. Young, "Waveguide integrated superconducting single-photon detectors implemented as near-perfect absorbers of coherent radiation," *Nat. Commun.* **6**(1), 8233 (2015).
13. J. P. Sprengers, A. Gaggero, D. Sahin, S. Jahanmirinejad, G. Frucci, F. Mattioli, R. Leoni, J. Beetz, M. Lerner, M. Kamp, S. Höfling, R. Sanjines, and A. Fiore, "Waveguide superconducting single-photon detectors for integrated quantum photonic circuits," *Appl. Phys. Lett.* **99**(18), 181110 (2011).
14. R. M. Heath, M. G. Tanner, T. D. Drysdale, S. Miki, V. Giannini, S. A. Maier, and R. H. Hadfield, "Nanoantenna enhancement for telecom-wavelength superconducting single photon detectors," *Nano Lett.* **15**(2), 819–822 (2015).
15. X. Hu, E. A. Dauler, R. J. Molnar, and K. K. Berggren, "Superconducting nanowire single-photon detectors integrated with optical nano-antennae," *Opt. Express* **19**(1), 17–31 (2011).
16. L. Novotny and B. Hecht, *Principles of Nano-Optics* (Cambridge University, 2006).
17. S. A. Maier, *Fundamentals and Applications Plasmonics: Fundamentals and Applications* (Springer, Heidelberg, 2004).
18. J. A. Schuller, E. S. Barnard, W. Cai, Y. C. Jun, J. S. White, and M. L. Brongersma, "Plasmonics for extreme light concentration and manipulation," *Nat. Mater.* **9**(3), 193–204 (2010).
19. N. J. Halas, S. Lal, W.-S. Chang, S. Link, and P. Nordlander, "Plasmons in strongly coupled metallic nanostructures," *Chem. Rev.* **111**(6), 3913–3961 (2011).
20. N. I. Landy, S. Sajuyigbe, J. J. Mock, D. R. Smith, and W. J. Padilla, "Perfect metamaterial absorber," *Phys. Rev. Lett.* **100**(20), 207402 (2008).
21. N. Liu, M. Mesch, T. Weiss, M. Hentschel, and H. Giessen, "Infrared perfect absorber and its application as plasmonic sensor," *Nano Lett.* **10**(7), 2342–2348 (2010).
22. A. Tittl, P. Mai, R. Taubert, D. Dregely, N. Liu, and H. Giessen, "Palladium-based plasmonic perfect absorber in the visible wavelength range and its application to hydrogen sensing," *Nano Lett.* **11**(10), 4366–4369 (2011).
23. A. Mukhtarova, L. Redaelli, D. Hazra, H. Machhadani, S. Lequien, M. Hofheinz, J.-L. Thomassin, F. Gustavo, J. Zichi, V. Zwiller, E. Monroy, and J.-M. Gérard, "Polarization-insensitive fiber-coupled superconducting-nanowire single photon detector using a high-index dielectric capping layer," *Opt. Express* **26**(13), 17697–17704 (2018).
24. P. Rath, O. Kahl, S. Ferrari, F. Sproll, G. Lewes-Malandrakis, D. Brink, K. Ilin, M. Siegel, C. Nebel, and W. Pernice, "Superconducting single-photon detectors integrated with diamond nanophotonic circuits," *Light Sci. Appl.* **4**(10), e338 (2015).
25. M. Hofherr, O. Wetzstein, S. Engert, T. Ortlev, B. Berg, K. Ilin, D. Henrich, R. Stolz, H. Toepfer, H.-G. Meyer, and M. Siegel, "Orthogonal sequencing multiplexer for superconducting nanowire single-photon detectors with RSFQ electronics readout circuit," *Opt. Express* **20**(27), 28683–28697 (2012).
26. S. Miki, T. Yamashita, H. Terai, and Z. Wang, "High performance fiber-coupled NbTiN superconducting nanowire single photon detectors with Gifford-McMahon cryocooler," *Opt. Express* **21**(8), 10208–10214 (2013).
27. L. You, J. Quan, Y. Wang, Y. Ma, X. Yang, Y. Liu, H. Li, J. Li, J. Wang, J. Liang, Z. Wang, and X. Xie, "Superconducting nanowire single photon detection system for space applications," *Opt. Express* **26**(3), 2965–2971 (2018).

28. I. Esmail Zadeh, J. W. N. Los, R. B. M. Gourgues, V. Steinmetz, G. Bulgarini, S. M. Dobrovolskiy, V. Zwiller, and S. N. Dorenbos, "Single-photon detectors combining high efficiency, high detection rates, and ultra-high timing resolution," *APL Photonics* **2**(11), 111301 (2017).
29. Y. P. Korneeva, M. Y. Mikhailov, Y. P. Pershin, N. N. Manova, A. V. Divochiy, Y. B. Vakhtomin, A. A. Korneev, K. V. Smirnov, A. G. Sivakov, A. Y. Devizenko, and G. N. Goltsman, "Superconducting single-photon detector made of MoSi film," *Supercond. Sci. Technol.* **27**(9), 095012 (2014).
30. V. B. Verma, B. Korzh, F. Bussi eres, R. D. Horansky, S. D. Dyer, A. E. Lita, I. Vayshenker, F. Marsili, M. D. Shaw, H. Zbinden, R. P. Mirin, and S. W. Nam, "High-efficiency superconducting nanowire single-photon detectors fabricated from MoSi thin-films," *Opt. Express* **23**(26), 33792–33801 (2015).
31. F. Marsili, V. B. Verma, J. A. Stern, S. Harrington, A. E. Lita, T. Gerrits, I. Vayshenker, B. Baek, M. D. Shaw, R. P. Mirin, and S. W. Nam, "Detecting single infrared photons with 93% system efficiency," *Nat. Photonics* **7**(3), 210–214 (2013).
32. A. J. Annunziata, D. F. Santavicca, J. D. Chudow, L. Frunzio, M. J. Rooks, A. Frydman, and D. E. Prober, "Niobium superconducting nanowire single-photon detectors," *IEEE Trans. Appl. Supercond.* **19**(3), 327-331 (2009).
33. S. Bagheri, N. Strohfeldt, M. Ubl, A. Berrier, M. Merker, G. Richter, M. Siegel, and H. Giessen, "Niobium as alternative material for refractory and active plasmonics," *ACS Photonics* **5**(8), 3298–3304 (2018).
34. T. Weiss, G. Granet, N. A. Gippius, S. G. Tikhodeev, and H. Giessen, "Matched coordinates and adaptive spatial resolution in the Fourier modal method," *Opt. Express* **17**(10), 8051–8061 (2009).
35. T. Weiss, N. A. Gippius, S. G. Tikhodeev, G. Granet, and H. Giessen, "Derivation of plasmonic resonances in the Fourier modal method with adaptive spatial resolution and matched coordinates," *J. Opt. Soc. Am. A* **28**(2), 238–244 (2011).
36. D. Tonini and C. Greggio, "Morphology of niobium films sputtered at different target–substrate Angle," *Proceeding of 11th workshop on RF superconductivity* (2003).
37. A. M. Valente-Feliciano, "Nb films: substrates, nucleation & crystal growth," *Proc. 15th Int. Conf. RF Supercond.* 332–342 (2011).
38. S. Bagheri, C. M. Zgrabik, T. Gissibl, A. Tittl, F. Sterl, R. Walter, S. De Zuani, A. Berrier, T. Stauden, G. Richter, E. L. Hu, and H. Giessen, "Large-area fabrication of TiN nanoantenna arrays for refractory plasmonics in the mid-infrared by femtosecond direct laser writing and interference lithography," *Opt. Mater. Express* **5**(11), 2625–2633 (2015).
39. S. Bagheri, H. Giessen, and F. Neubrech, "Large-area antenna-assisted SEIRA substrates by laser interference lithography," *Adv. Opt. Mater.* **2**(11), 1050–1056 (2014).
40. S. Bagheri, N. Strohfeldt, F. Sterl, A. Berrier, A. Tittl, and H. Giessen, "Large-area low-cost plasmonic perfect absorber chemical sensor fabricated by laser interference lithography," *ACS Sens.* **1**(9), 1148–1154 (2016).
41. R. Walter, A. Tittl, A. Berrier, F. Sterl, T. Weiss, and H. Giessen, "Large-area low-cost tunable plasmonic perfect absorber in the near infrared by colloidal etching lithography," *Adv. Opt. Mater.* **3**(3), 398–403 (2015).